ISSN 1674-1056
http://cpb.iphy.ac.cn
http://iopscience.iop.org/cpb
中国物理 B
Chinese Physics
中国物理 Chinese Physics B

Transmission properties of microwave in rectangular waveguide through argon plasma

Xiaoyu Han(韩晓宇), Dawei Li(李大伟), Meie Chen(陈美娥), Zhan Zhang(张展), Zheng Li(李铮), Yujian Li(李雨键), Junhong Wang(王均宏)

Citation: Chin. Phys. B . 2019, 28(3): 035204. **doi:** 10.1088/1674-1056/28/3/035204
Journal homepage: http://cpb.iphy.ac.cn; http://iopscience.iop.org/cpb

What follows is a list of articles you may be interested in

Similarity principle of microwave argon plasma at low pressure

Xiao-Yu Han(韩晓宇), Jun-Hong Wang(王均宏), Mei-E Chen(陈美娥), Zhan Zhang(张展), Zheng Li(李铮), Yu-Jian Li(李雨键)

Chin. Phys. B . 2018, 27(8): 085206. **doi:** 10.1088/1674-1056/27/8/085206

Preparation of Se-based solar cell using spin-coating method in ambient condition

Menghua Zhu(朱孟花), Yaxin Deng(邓雅心), Weiwei Liu(刘伟伟), Xin Li(李欣)

Chin. Phys. B . 2018, 27(1): 015202. **doi:** 10.1088/1674-1056/27/1/015202

Initial growth and microstructure feature of Ag films prepared by very-high-frequency magnetron sputtering

Yue Zhang(张悦), Chao Ye(叶超), Xiang-Ying Wang(王响英), Pei-Fang Yang(杨培芳), Jia-Min Guo(郭佳敏), Su Zhang(张苏)

Chin. Phys. B . 2017, 26(9): 095206. **doi:** 10.1088/1674-1056/26/9/095206

Effect of driving frequency on the structure of silicon grown on Ag (111) films by very-high-frequency magnetron sputtering

Jia-Min Guo(郭佳敏), Chao Ye(叶超), Xiang-Ying Wang(王响英), Pei-FangYang(杨培芳), Su Zhang(张苏)

Chin. Phys. B . 2017, 26(6): 065207. **doi:** 10.1088/1674-1056/26/6/065207

Tunable terahertz plasmon in grating-gate coupled graphene with a resonant cavity

Yan Bo, Yang Xin-Xin, Fang Jing-Yue, Huang Yong-Dan, Qin Hua, Qin Shi-Qiao

Chin. Phys. B . 2015, 24(1): 015203. **doi:** 10.1088/1674-1056/24/1/015203

Transmission properties of microwave in rectangular waveguide through argon plasma*

Xiaoyu Han(韩晓宇)[1], Dawei Li(李大伟)[2], Meie Chen(陈美娥)[1], Zhan Zhang(张展)[1], Zheng Li(李铮)[1], Yujian Li(李雨键)[1], and Junhong Wang(王均宏)[1,†]

[1] *Institude of Lightwave Technology, Beijing Jiaotong University, Beijing* 100044, *China*
[2] *China Academy of Launch Vehicle Technology, Beijing* 100076, *China*

(Received 24 October 2018; revised manuscript received 7 January 2019; published online 26 February 2019)

To study the impact of plasma generated by microwave breakdown on the propagation properties of microwave in high power microwave (HPM) devices, a three-dimensional (3-D) fluid model of argon plasma slab in rectangular waveguide is established and calculated by the finite-difference-time-domain (FDTD) method. A rectangular waveguide with a breakdown chamber filled with argon is set as the physics model, and HPM with frequency of 3–50 GHz propagates through this physics model. The time evolutions of the breakdown process are investigated, the reflection, transmission, and absorption coefficients of HPM are calculated, and the influences of some important parameters, including the thickness of the plasma slab and the microwave frequency on the propagation properties of the microwave are shown. Results of this work can offer theoretical instructions for suppressing the influence of breakdown to the performance of HPM devices, and for the use of microwave breakdown, such as the design of plasma limiter or absorber in HPM devices.

Keywords: high power microwave, argon plasma, propagation properties, finite-difference-time-domain (FDTD) method

PACS: 52.80.Pi, 52.65.–y, 51.50.+v, 52.50.Sw **DOI:** 10.1088/1674-1056/28/3/035204

1. Introduction

With the development of high power microwave (HPM) source technology, the strength of electric field transmitted in microwave devices is getting closer and closer to the breakdown threshold of the background gas, and breakdown will take place with a large probability. On one hand, plasma generated by microwave breakdown will become a dominant factor which influences the performance of HPM devices.[1–4] On the other hand, more works concerning the plasma generated by microwave breakdown as absorbers or limiters of HPM in microwave devices are reported, which can be seen as the rational use of the influence of plasma on the microwave propagation properties.[5–9] No matter what we concern about, predicting and suppressing the influence of breakdown or making use of breakdown, a realistic and accurate model is necessary to obtain the accurate key parameters of the microwave plasma and to study the propagation properties of HPM in the plasma efficiently.

A number of investigations of the interaction between plasma and the HPM transmitted through it have been presented. Laroussi and Roth investigated the electromagnetic (EM) wave propagation through a non-uniform plasma slab by using Fresnel reflection coefficients.[10] Using scattering matrix method (SMM), Tang *et al.* analyzed the broadband absorption characteristics of the magnetized non-uniform plasma.[11] Jazi *et al.* provided an analytical method to study the reflection and absorption of EM waves in an inhomogeneous dissipative magnetized plasma slab, and also discussed the effects of the external magnetic field, the frequency of the incident wave, and the electron thermal velocity.[12] Most of these works considered only the steady-state plasmas with constant collision frequency, constant electron frequency, and certain distribution of electron density, and treated them as dielectric slabs with specific parameters. Recently, Liao *et al.* used the effective electron diffusion coefficient and empirical time-varying frequency coefficients to improve the accuracy of the fluid model and studied the interaction of high-power microwave with air breakdown plasma.[13] In this paper, a three-dimensional (3-D) time-varying plasma model based on Ref. [13] is proposed for obtaining more accurate and factual distributions of the key parameters, and studying the propagating properties of the HPM.

2. Model and method

Very detailed one-dimensional and two-dimensional fluid models to study the propagation of HPM through gas have been reported by Zhao *et al.*,[1,13–15] which consist of electron fluid equations, Maxwell's equations, and the definition of transport coefficients. The 3-D fluid model in this paper is a direct generalization of their models.

*Project supported by the National Natural Science Foundation of China (Grant No. 61331002).
†Corresponding author. E-mail: wangjunh@bjtu.edu.cn
© 2019 Chinese Physical Society and IOP Publishing Ltd

2.1. Physics model

Figure 1 shows the 3-D schematic of waveguide and the cross section of breakdown environment in yz plane. The waveguide used in this paper is the standard BJ-22 type, whose width and height are $a = 108$ mm and $b = 54$ mm, respectively. The waveguide is assumed to be filled with three layers of media: an argon chamber sandwiched by two quartz walls, as shown in Fig. 1(b). The argon is under atmospheric pressure, and the length of the argon chamber is $p = 15$ mm in regular study, and varies from 5 mm to 25 mm when studying the influence of the thickness of the plasma slab. For the incident HPM, the amplitude of the electric field is set to 10^6 V/m, and its frequency is 3 GHz in regular study, and ranges from 3 GHz to 50 GHz when studying the influence of the microwave frequency. The initial electron density and initial mean electron energy are set to 10^9 m^{-3} and 0 eV, respectively. HPM incidents from the left port and propagates through the whole waveguide, but discharge occurs only in the argon chamber and plasma generated by HPM will be blocked in this chamber.

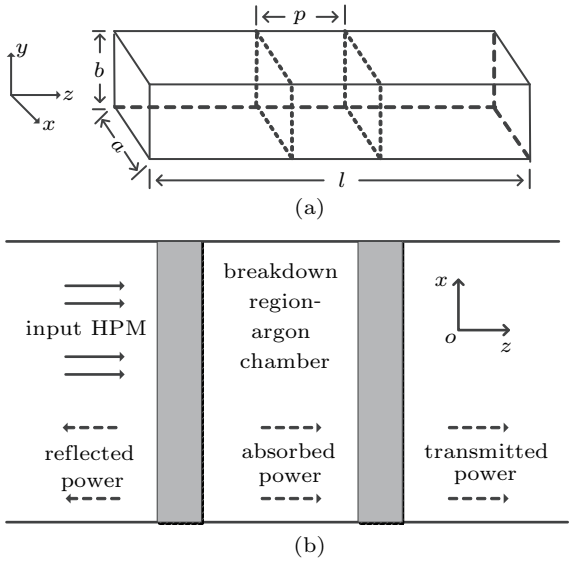


Fig. 1. Schematic of waveguide and breakdown area used in this paper: (a) 3-D scheme, (b) cross section scheme of xz plane.

The basic reactions of argon breakdown in the chamber include:[16–18] (R1, elastic collision) $e + Ar => e + Ar$, (R2, excitation) $e + Ar => e + Ar^*$, (R3, ionization by single collision) $e + Ar => 2e + Ar^+$, and (R4, stepwise ionization) $e + Ar^* => 2e + Ar^+$, of which the different excited levels of argon atoms are combined for simplicity.

2.2. Fluid model of plasma

The equations of the electron fluid model for plasma can be written as[14,15]

$$\frac{\partial E_x}{\partial t} + \frac{\sigma}{\varepsilon_0}E_x = \frac{1}{\varepsilon_0}\left(\frac{\partial H_z}{\partial y} - \frac{\partial H_y}{\partial z}\right) - \frac{1}{\varepsilon_0}N_e u_x q_e, \tag{1}$$

$$\frac{\partial E_y}{\partial t} + \frac{\sigma}{\varepsilon_0}E_y = \frac{1}{\varepsilon_0}\left(\frac{\partial H_x}{\partial z} - \frac{\partial H_z}{\partial x}\right) - \frac{1}{\varepsilon_0}N_e u_y q_e, \tag{2}$$

$$\frac{\partial E_z}{\partial t} + \frac{\sigma}{\varepsilon_0}E_z = \frac{1}{\varepsilon_0}\left(\frac{\partial H_y}{\partial x} - \frac{\partial H_x}{\partial y}\right) - \frac{1}{\varepsilon_0}N_e u_z q_e, \tag{3}$$

$$-\mu_0\frac{\partial H_x}{\partial t} - \sigma_m H_x = \frac{\partial E_z}{\partial y} - \frac{\partial E_y}{\partial z}, \tag{4}$$

$$-\mu_0\frac{\partial H_y}{\partial t} - \sigma_m H_y = \frac{\partial E_x}{\partial z} - \frac{\partial E_z}{\partial x}, \tag{5}$$

$$-\mu_0\frac{\partial H_z}{\partial t} - \sigma_m H_z = \frac{\partial E_y}{\partial x} - \frac{\partial E_x}{\partial y}, \tag{6}$$

$$\frac{\partial N_e}{\partial t} = (\nu_i - \nu_a)N_e - \frac{\partial(N_e u_x)}{\partial x} - \frac{\partial(N_e u_y)}{\partial y} - \frac{\partial(N_e u_z)}{\partial z}, \tag{7}$$

$$\frac{\partial(N_e u_x)}{\partial t} = \frac{q_e}{m_e}N_e E_x + \frac{q_e}{m_e}N_e\mu_0 u_y H_z - \frac{q_e}{m_e}N_e\mu_0 u_z H_y - \nu_c N_e u_x, \tag{8}$$

$$\frac{\partial(N_e u_y)}{\partial t} = \frac{q_e}{m_e}N_e E_y + \frac{q_e}{m_e}N_e\mu_0 u_z H_x - \frac{q_e}{m_e}N_e\mu_0 u_x H_z - \nu_c N_e u_y, \tag{9}$$

$$\frac{\partial(N_e u_z)}{\partial t} = \frac{q_e}{m_e}N_e E_z + \frac{q_e}{m_e}N_e\mu_0 u_x H_y - \frac{q_e}{m_e}N_e\mu_0 u_y H_x - \nu_c N_e u_z, \tag{10}$$

$$\frac{\partial(N_e\bar{\varepsilon}_e)}{\partial t} = q_e(N_e u_x E_x + N_e u_z E_z) - N_e Q_l, \tag{11}$$

where E_x, E_y, and E_z are the electric field components along the x, y, and z axes, H_x, H_y, and H_z are the magnetic field components along the x, y, and z axes, u_x, u_y, and u_z are the electron velocities along the x, y, and z axes, respectively, N_e is the electron density, q_e and m_e are the charge and mass of one electron, respectively, ε_0 and μ_0 are the permittivity and permeability of free space, respectively, and ν_i, ν_a, ν_m, and Q_l are the ionization frequency, attachment frequency, collision frequency , and energy loss frequency, respectively, ε_e is the mean electron energy. The finite-difference-time-domain (FDTD) numerical scheme proposed in Refs. [13] and [14] is employed to solve the equations above.

The electron energy-dependent transport coefficients are defined as[14]

$$\nu_i = N_{Ar}\cdot\int_{\varepsilon_{Ar-4}}^{\infty}\sqrt{\frac{2\varepsilon_e}{m_e}}\sigma_{Ar-4}(\varepsilon_e)f(\varepsilon_e)\,d\varepsilon_e, \tag{12}$$

$$\nu_m = N_{Ar}\cdot\int_{\varepsilon_{Ar-1}}^{\infty}\sqrt{\frac{2\varepsilon_e}{m_e}}\sigma_{Ar-1}(\varepsilon_e)f(\varepsilon_e)\,d\varepsilon_e, \tag{13}$$

$$\nu_l = \nu_{el} + \nu_{inel}, \tag{14}$$

where ε_{Ar-n} and σ_{Ar-n} are the energy threshold and cross section data of the n-th reaction of the reaction list of argon, ν_{el} and ν_{inel} are the energy loss coefficients caused by elastic collisions and inelastic collisions, respectively, and are defined as

$$\nu_{el} = N_{Ar}\frac{8}{3\sqrt{\pi}}\frac{m_e}{M_{Ar}}\cdot\int_{\varepsilon_{Ar-1}}^{\infty}\sqrt{\frac{2\varepsilon_e}{m_e}}\sigma_{Ar-1}(\varepsilon_e)f(\varepsilon_e)\,d\varepsilon_e, \tag{15}$$

$$\nu_{inel} = N_{Ar}\sum_{j=Ar-2}^{Ar-7}\int_{\varepsilon_j}^{\infty}\sqrt{\frac{2\varepsilon_e}{m_e}}\sigma_j f(\varepsilon_e)\,d\varepsilon_e, \tag{16}$$

$N_{\rm Ar}$ is the density of argon and is given by

$$N_{\rm Ar}(\rm m^{-3}) = \frac{p(\rm Pa)}{k\cdot T(\rm K)}, \tag{17}$$

$f(\varepsilon_{\rm e})$ is the reduced electron energy distribution function (EEDF) for argon, and k, T, and p are the Boltzmann constant, temperature of gas, and pressure of gas, respectively. All the transport coefficients above will update with the changing electron energy.

The modified EEDF used in this paper can be written as[19,20]

$$f(\varepsilon_{\rm e}) = \frac{\chi}{\bar{\varepsilon}_{\rm e}^{3/2}} \frac{\left[\Gamma\left(\frac{5}{2\chi}\right)\right]^{3/2}}{\left[\Gamma\left(\frac{3}{2\chi}\right)\right]^{5/2}} \varepsilon_{\rm e}^{1/2} \exp\left\{-\left[\frac{\Gamma\left(\frac{5}{2\chi}\right)}{\Gamma\left(\frac{3}{2\chi}\right)}\frac{\varepsilon_{\rm e}}{\bar{\varepsilon}_{\rm e}}\right]^{\chi}\right\}, \tag{18}$$

$$\Gamma(\xi) = \int_0^{\infty} t^{\xi-1}\exp(-{\rm t})\,{\rm dt}, \quad \xi > 0, \tag{19}$$

where χ has been calculated to be 6.5 for argon at atmosphere pressure by particle in cell (PIC) simulation.[19]

2.3. The 3-D difference iteration scheme of FDTD method

The 3-D FDTD scheme is expanded from the 2-D scheme proposed in Ref. [13] and is employed in this paper to calculate all the unknowns in Eqs. (1)–(19). For the convenient calculation of parameters u_x, u_y, u_z, and $u_{\rm e}$, replacement factors are defined in this paper as $U_x = N_{\rm e}u_x$, $U_y = N_{\rm e}u_y$, $U_z = N_{\rm e}u_z$, $U_{\rm e} = N_{\rm e}\varepsilon_{\rm e}$. Components E_x, E_y, E_z, $N_{\rm e}$, and $U_{\rm e}$ are set at the integral grids, and H_x, H_y, H_z, U_x, U_y, and U_z are set at the half integral-grids.

Taking equations of partial E_x, H_x, $N_{\rm e}$, $\varepsilon_{\rm e}$, and u_x as the example, the difference iteration scheme of the FDTD method can be written as

$$\begin{aligned}
&E_x^{n+1}\left(i+\frac{1}{2},j,k\right)\\
&= \frac{\varepsilon_0/\Delta t-\sigma/2}{\varepsilon_0/\Delta t+\sigma/2}E_x^{n}\left(i+\frac{1}{2},j,k\right) + \frac{1}{\varepsilon_0/\Delta t+\sigma/2}\\
&\times\left[\frac{H_z^{n+1/2}(i+\frac{1}{2},j+\frac{1}{2},k)-H_z^{n+1/2}(i+\frac{1}{2},j-\frac{1}{2},k)}{\Delta y}\right.\\
&-\frac{H_y^{n+1/2}(i+\frac{1}{2},j,k+\frac{1}{2})-H_y^{n+1/2}(i+\frac{1}{2},j,k-\frac{1}{2})}{\Delta z}\\
&\left.-q_{\rm e}u_x^{n+1/2}\left(i+\frac{1}{2},j,k\right)\right],
\end{aligned} \tag{20}$$

$$\begin{aligned}
&H_x^{n+3/2}\left(i,j+\frac{1}{2},k+\frac{1}{2}\right)\\
&= \frac{\mu_0/\Delta t-\sigma_{\rm m}/2}{\mu_0/\Delta t+\sigma_{\rm m}/2}H_x^{n+1/2}\left(i,j+\frac{1}{2},k+\frac{1}{2}\right)\\
&-\frac{1}{\mu_0/\Delta t+\sigma_{\rm m}/2}\left[\frac{E_z^{n}(i,j+\frac{1}{2},k)-E_z^{n}(i,j-\frac{1}{2},k)}{\Delta y}\right.\\
&\left.-\frac{E_y^{n}(i,j,k+\frac{1}{2})-E_y^{n}(i,j,k-\frac{1}{2})}{\Delta z}\right],
\end{aligned} \tag{21}$$

$$\begin{aligned}
&N_{\rm e}^{n+1}(i,j,k)\\
&= \frac{1/\Delta t+(\nu_{\rm i}-\nu_{\rm a})/2}{1/\Delta t-(\nu_{\rm i}-\nu_{\rm a})/2}N_{\rm e}^{n}(i,j,k)\\
&-\frac{1}{1/\Delta t-(\nu_{\rm i}-\nu_{\rm a})/2}\\
&\times\left[\frac{U_x^{n+1/2}(i+\frac{1}{2},j,k)-U_x^{n+1/2}(i-\frac{1}{2},j,k)}{\Delta x}\right.\\
&+\frac{U_y^{n+1/2}(i,j+\frac{1}{2},k)-U_y^{n+1/2}(i,j-\frac{1}{2},k)}{\Delta y}\\
&\left.+\frac{U_z^{n+1/2}(i,j,k+\frac{1}{2})-U_z^{n+1/2}(i,j,k-\frac{1}{2})}{\Delta z}\right],
\end{aligned} \tag{22}$$

With the introduction of the replacement factors, $\varepsilon_{\rm e}$ and μ_x can be calculated by

$$\begin{aligned}
&U_{\rm e}^{n+1}(i,j,k)\\
&= U_{\rm e}^{n}(i,j,k)+q_{\rm e}\Delta t\left[\frac{E_x^{n+1/2}(i+\frac{1}{2},j,k)+E_x^{n+1/2}(i-\frac{1}{2},j,k)}{2}\right.\\
&\times\frac{U_x^{n+1/2}(i+\frac{1}{2},j,k)+U_x^{n+1/2}(i-\frac{1}{2},j,k)}{2}\\
&+\frac{E_y^{n+1/2}(i,j+\frac{1}{2},k)+E_y^{n+1/2}(i,j-\frac{1}{2},k)}{2}\\
&\times\frac{U_y^{n+1/2}(i,j+\frac{1}{2},k)+U_y^{n+1/2}(i,j-\frac{1}{2},k)}{2}\\
&+\frac{E_z^{n+1/2}(i,j,k+\frac{1}{2})+E_z^{n+1/2}(i,j,k-\frac{1}{2})}{2}\\
&\left.+\frac{U_z^{n+1/2}(i,j,k+\frac{1}{2})+U_z^{n+1/2}(i,j,k-\frac{1}{2})}{2}\right]\\
&-\frac{N_{\rm e}^{n+1}(i,j,k)+N_{\rm e}^{n}(i,j,k)}{2}\nu_{\rm l}\Delta t,
\end{aligned} \tag{23}$$

$$\begin{aligned}
&U_x^{n+3/2}\\
&= \frac{(AE+CF)(A^2+D^2)-(AG-DF)(AB-CD)}{(A^2+C^2)(A^2+D^2)+(AB+CD)(AB-CD)},
\end{aligned} \tag{24}$$

where

$$A = \frac{1}{\Delta t}+\frac{\nu_{\rm c}}{2}, \tag{25}$$

$$B = \frac{q_{\rm e}\mu_0}{m_{\rm e}}(H_y^{n+3/2}+H_y^{n+1/2}), \tag{26}$$

$$C = \frac{q_{\rm e}\mu_0}{m_{\rm e}}(H_z^{n+3/2}+H_z^{n+1/2}), \tag{27}$$

$$D = \frac{q_{\rm e}\mu_0}{m_{\rm e}}(H_x^{n+3/2}+H_x^{n+1/2}), \tag{28}$$

$$\begin{aligned}
E &= \left(\frac{1}{\Delta t}-\frac{\nu_{\rm c}}{2}\right)U_x^{n+1/2}+\frac{q_{\rm e}}{m_{\rm e}}N_{\rm e}^{n+1}E_x^{n+1}\\
&+\frac{q_{\rm e}\mu_0}{2m_{\rm e}}H_z^{n+1}U_y^{n+1/2}-\frac{q_{\rm e}\mu_0}{2m_{\rm e}}H_y^{n+1}U_z^{n+1/2},
\end{aligned} \tag{29}$$

$$\begin{aligned}
F &= \left(\frac{1}{\Delta t}-\frac{\nu_{\rm c}}{2}\right)U_y^{n+1/2}+\frac{q_{\rm e}}{m_{\rm e}}N_{\rm e}^{n+1}E_y^{n+1}\\
&-\frac{q_{\rm e}\mu_0}{2m_{\rm e}}H_z^{n+1}U_x^{n+1/2}+\frac{q_{\rm e}\mu_0}{2m_{\rm e}}H_x^{n+1}U_z^{n+1/2},
\end{aligned} \tag{30}$$

$$G = \left(\frac{1}{\Delta t}-\frac{\nu_{\rm c}}{2}\right)U_z^{n+1/2}+\frac{q_{\rm e}}{m_{\rm e}}N_{\rm e}^{n+1}E_z^{n+1}$$

$$+\frac{q_e\mu_0}{2m_e}H_y^{n+1}U_x^{n+1/2}-\frac{q_e\mu_0}{2m_e}H_x^{n+1}U_y^{n+1/2}. \quad (31)$$

Electron energy ε_e calculated by Eq. (23) on every step is substituted into Eqs. (12)–(19) to update the transmission coefficients and EEDF.

3. Results and discussion

3.1. Validation of the model and method

To validate the proposed fluid model, the comparison of breakdown thresholds between experimental data and the predictions of our work at 3 GHz is shown in Fig. 2. It is observed that the breakdown thresholds calculated by this work are quite close to Krasik's experimental data at 3 GHz[21] and MacDonald's experimental data at 2.85 GHz.[22]

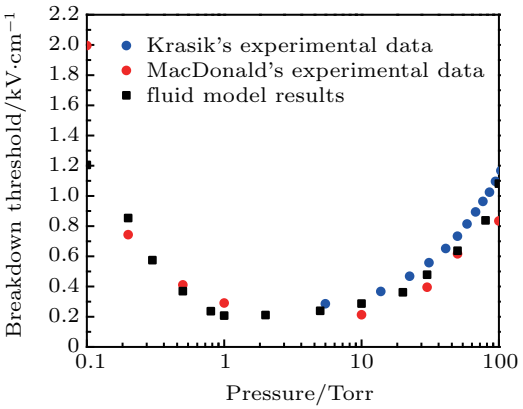


Fig. 2. Comparison between experimental data and results of our work.

3.2. Time evolution of breakdown process

The time evolutions of the electric field and electron density at the center of the plasma slab ($x = 54$ mm, $y = 27$ mm, $z = 5$ mm) are shown in Fig. 3. HPM with power higher than the threshold of argon breakdown brings up the gas discharge, the electron density keeps growing and gets steady at around 16 ns, and reaches the peak value of 4.21×10^{18} m^{-3} . Taking the electron density 10^8 times higher than the initial value as the criterion, then the breakdown time is 14 ns. From the curve of the electric field, it can be observed that the increased electron density in the chamber leads to the obvious reduction of the electric field.

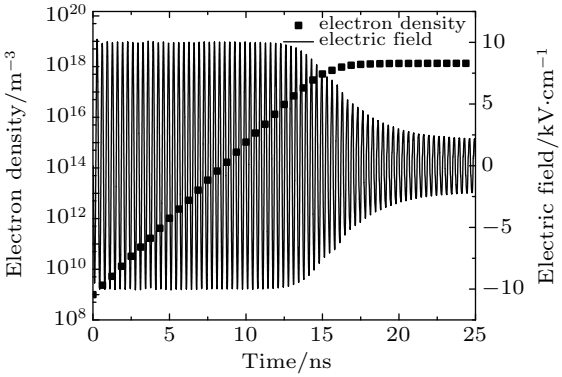


Fig. 3. Time evolutions of the electric field and electron density in the center of the plasma slab.

Benefiting from the establishment of this model, 3-D distributions of electron density and electric field can be shown. The results at different breakdown stages are shown in Figs. 4 and 5. It is observed that before the breakdown (0.1 ns), few argon atoms are ionized, and the maximum electron density is around 1.16×10^9 m^{-3}. The distribution of the electric field is not affected and the waveguide works in TE_{10} mode. At the beginning of the breakdown process (10 ns), plasma with density around

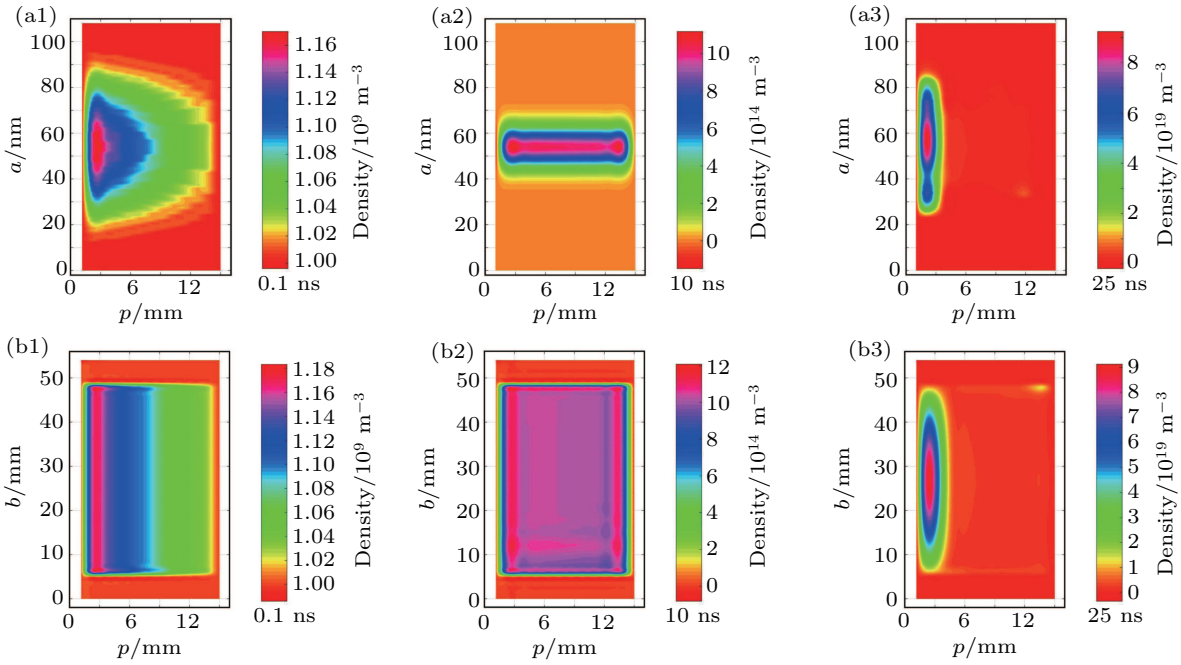


Fig. 4. Distributions of electron density in breakdown area at different time: (a) on xz plane, $y = 27$ mm, (b) on yz plane, $x = 54$ mm.

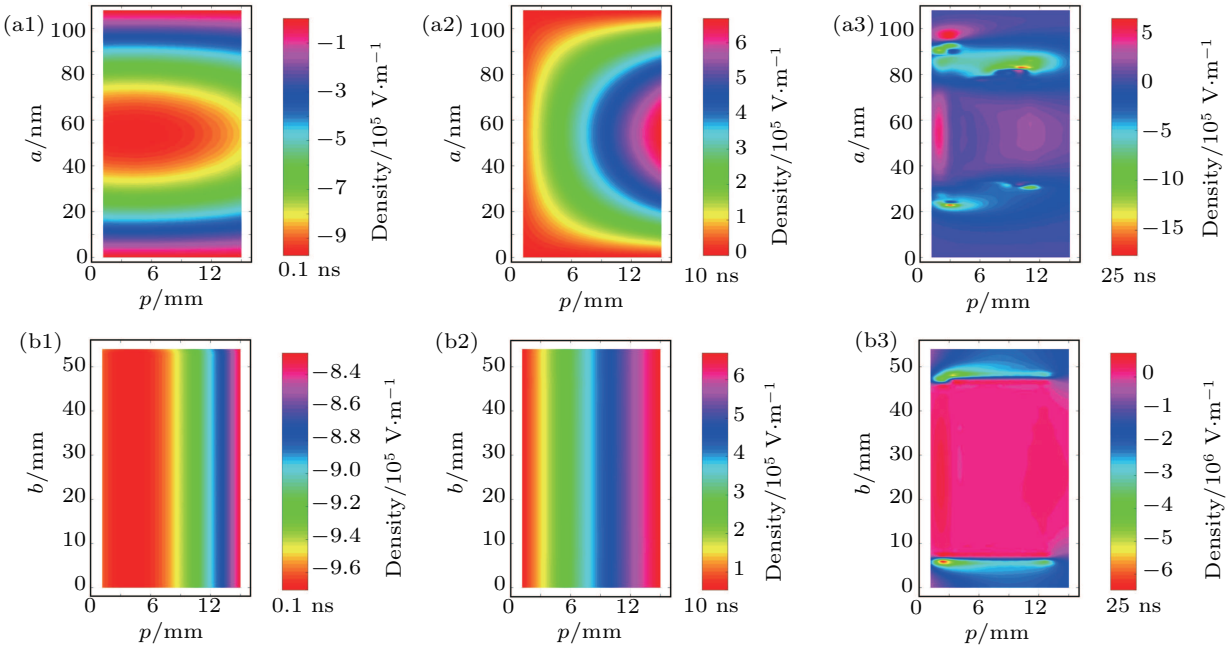


Fig. 5. Distributions of electric field in breakdown area at different time: (a) on xz plane, $y = 27$ mm, (b) on yz plane, $x = 54$ mm.

1×10^{15} m^{-3} is generated in the high electric field region. The maximum electric field is reduced from about 1×10^6 V/m to about 6×10^5 V/m, which means that the plasma begins to reflect and absorb the microwave. At the late stage of breakdown (25 ns), the argon plasma is concentrated to the incident terminal of the waveguide and becomes steady. When the density of plasma reaches around 9×10^{19} m^{-3} , the plasma frequency is higher than the frequency of the incident HPM, so the real part of plasma's permittivity becomes negative, HPM can no longer propagate through plasma and the incident energy is blocked at the input terminal of the waveguide. As a result, argon atoms in the rest part of the waveguide only obtain very limited energy, and cannot be ionized.

3.3. Propagation properties of microwave in plasma

The transmission coefficient C_t, reflection coefficient C_r, and absorption coefficient C_a in one period are calculated by

$$C_r = \frac{\frac{1}{T}\int_{t-T}^{T}\oint_{S_1}(|\boldsymbol{E}_1|)^2 \mathrm{d}S_1}{\frac{1}{T}\int_{t-T}^{T}\oint_{S_1}(|\boldsymbol{E}_{\mathrm{ref}}|)^2 \mathrm{d}S_1}, \tag{32}$$

$$C_t = \frac{\frac{1}{T}\int_{t-T}^{T}\oint_{S_2}(|\boldsymbol{E}_2|)^2 \mathrm{d}S_2}{\frac{1}{T}\int_{t-T}^{T}\oint_{S_1}(|\boldsymbol{E}_{\mathrm{ref}}|)^2 \mathrm{d}S_2}, \tag{33}$$

$$C_a = 1 - C_t - C_r, \tag{34}$$

where $\boldsymbol{E}_1$ and $\boldsymbol{E}_2$ are the reflected and transmitted electric fields on surfaces S_1 and S_2, and S_1 and S_2 are the waveguide cross sections in front of and behind the argon chamber, respectively. $\boldsymbol{E}_{\mathrm{ref}}$ is the electric field for reference, which is the electric field on the corresponding surfaces when the same incident microwave is fed into the waveguide but without plasma.

Figure 6 shows the propagation properties of HPM in plasma and the mean electron density on the incident surface of the breakdown region, which indicates the performance of the plasma to HPM. Using the electron density in this figure as the judgement basis, before the gas discharge occurs (before 12 ns), most of the energy passes through the gas chamber, and about 28% of the energy is absorbed, which provides energy to accelerate the electrons. Through the collision between the accelerated electrons and other particles, these absorbed microwave energy is transferred into the mean electron energy to provide energy for the reactions in breakdown, and the reflection at this time is quite weak, this can be explained by the following equation:[23]

$$\varepsilon_r = 1 - \frac{\omega_p^2}{f^2 + v^2} - \mathrm{j}\frac{\omega_p^2 \cdot v}{\omega(\omega^2 + v^2)}, \tag{35}$$

where ε_r is the complex relative permittivity of plasma, ω_p is the plasma frequency, f is the microwave frequency, and v is the plasma collision frequency. Before the occurrence of

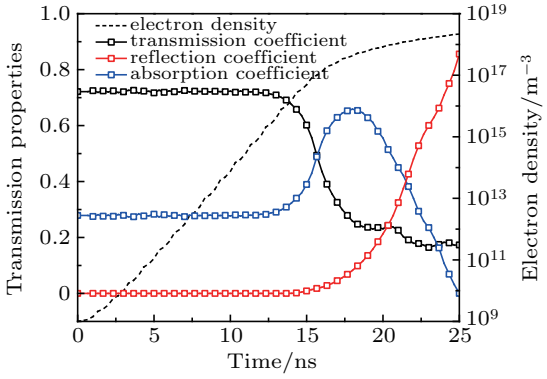


Fig. 6. Propagation properties of HPM in plasma.

discharge, the value of ω_p is quite small with a low electron density, and $\varepsilon_r \approx 1$. During the breakdown process (12–20 ns), the mean electron energy gets higher, which increases the ionization and results in higher electron density. The plasma generated in this process reflects and absorbs the incident power. Finally (after 20 ns), the high-density plasma is generated, the transmission and absorption coefficients become very low, and the HPM is almost totally reflected.

3.4. The influence of the frequency of microwave

Figure 7 shows the influence of the microwave frequency on the propagation properties of microwave in plasma. Comparing the curves in Fig. 5, it can be observed that the reflection coefficient at $f = 3$ GHz is larger than those at other frequencies after 15 ns, which means that high density plasma has been generated. The maximum absorption coefficient occurs during 14–22 ns when $f = 10$ GHz, as shown in Fig. 5(c), which can be explained by the equation of plasma frequency $f_p = (n_e e^2/m_e \varepsilon_0)^{1/2}/2\pi$, where f_p is the plasma frequency which is calculated to be approximately 10 GHz in this model when the mean electron density is about 1.2×10^{18} m^{-3}. So when the frequency of the incident microwave is around 10 GHz, the particles of plasma will resonate with the microwave, and the energy of the microwave will be transferred into the kinetic energy of the particles very quickly, leading to the maximum absorption coefficient. With the frequency increasing, the reflection and absorption decrease, when $f =$ 50 GHz, the frequency of the incident microwave is considerably higher than the plasma frequency, and then most of the energy passing through the plasma.

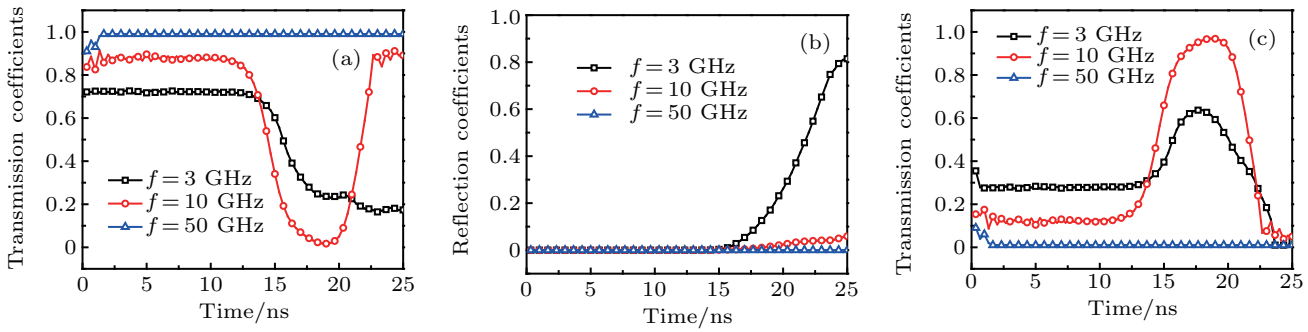


Fig. 7. Influence of the microwave frequency on the propagation properties of HPM in plasma: (a) transmission coefficients, (b) reflection coefficients, (c) absorption coefficients.

3.5. The influence of the thickness of plasma slab

In Fig. 8, the influence of the thickness of the plasma slab on the propagation properties of HPM in plasma is shown. From this figure, we can see that when the plasma slab is only 5 mm in thickness, the mean electron density of the whole plasma slab is about 1×10^{18} m^{-3}, and only 18% energy can be transmitted, when the plasma slab is only 25 mm in thickness, nearly all the energy is reflected and absorbed. These results show the possibility and the efficiency of making use of the microwave plasma as limiter or absorber in HPM devices.

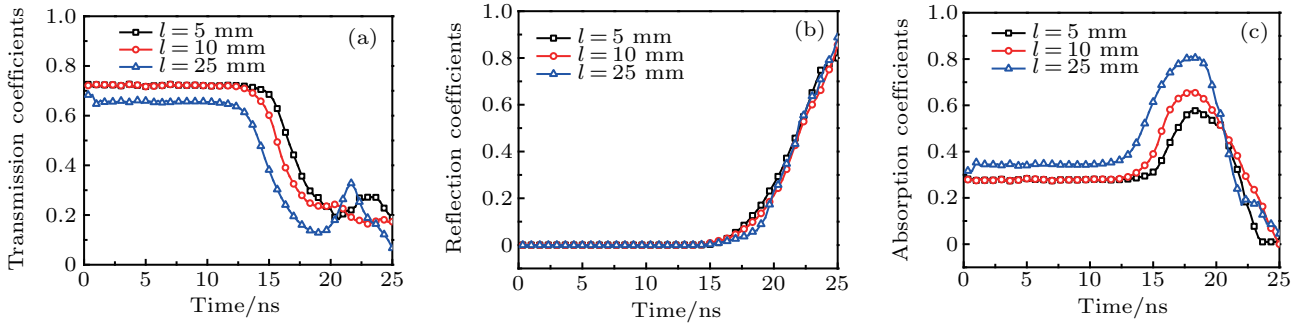


Fig. 8. Influence of the thickness of the plasma slab on the propagation properties of HPM in plasma: (a) transmission coefficients, (b) reflection coefficients, (c) absorption coefficients.

4. Conclusion

In this paper, a 3-D fluid model of plasma slab in rectangular waveguide is proposed and solved by the FDTD method. The detailed breakdown process can be shown and the accurate distributions of all important parameters of plasma can be obtained by this 3-D model. The influences of microwave frequency and the thickness of plasma slab on the propagation properties are also studied. This work can not only provide a 3-D model for studying the breakdown process, but can also offer instructions for the design of plasma-based HPM devices,

such as the limiters and the absorbers.

References

[1] Zhao P C, Guo L X and Shu P P 2016 *Phys. Plasmas* **23** 092105
[2] Xiao W and Huang K M 2016 *IEEE Trans. Plasma Sci.* **44** 1075
[3] Kim H C and Verboncoeur J P 2007 *Comput. Phys. Commun.* **177** 118
[4] Hu B J, Wei G, and Lai S L 1999 *IEEE Trans. Plasma Sci.* **27** 1131
[5] Qian C, Ding D Z, Fan Z H and Chen R S 2015 *Phys. Plasmas* **22** 032111
[6] Ji J Z, Ma Y P and Guo N 2018 *Optik* **165** 240
[7] Robert and Vidmar 1990 *IEEE Trans. Plasma Sci.* **18** 733
[8] Qian C, Ding D Z, Bi J J and Chen R S 2016 *IEEE Microwave and Wireless Components Letters* **26** 77
[9] Mankowski J, Hemmert D, Neuber A and Krompholz H 2002 *IEEE Trans. Plasma Sci.* **30** 102
[10] Laroussi M and Roth J R 1993 *IEEE Trans. Plasma Sci.* **21** 366
[11] Tang D L, Sun A P, Qiu X M and Chu P K 2003 *IEEE Trans. Plasma Sci.* **31** 405
[12] Jazi B and Mehdiam H 2004 *Plasma Phys. Control. Fusion* **46** 507
[13] Zhao P C, Liao C and Lin W 2011 *J. Electromagn. Waves Appl.* **25** 2365
[14] Zhao P C, Liao C, Lin W B, Chang L and Fu H J 2011 *Phys. Plasmas* **18** 102111
[15] Zhao P C, Guo L X and Li H M 2015 *Chin. Phys. B* **24** 105102
[16] Fu Y Y, Verboncoeur J P, Christlieb A J and Wang X X 2017 *Phys. Plasmas* **24** 083516
[17] Fu Y Y, Luo H Y, Zou X B and Wang X X 2014 *IEEE Trans. Plasma Sci.* **42** 1544
[18] Zhang L, He F, Li S C and Ouyang J T 2013 *Chin. Phys. B* **22** 125202
[19] Nam S K and Verboncoeur J P 2008 *Appl. Phys. Lett.* **92** 231502
[20] Nam S K and Verboncoeur J P 2008 *Appl. Phys. Lett.* **93** 151504
[21] Krasik S, Alpert D and McCoubrey O 1949 *Phys. Rev.* **76** 722
[22] MacDonald A 1966 *Microwave Breakdown in Gases* (New York: Wiley)
[23] Soliman E A, Helaly A and Megahed A A 2007 *Prog. Electromagn. Res.* **67** 25